Progress in Nuclear Energy 52 (2010) 84–96

Contents lists available at ScienceDirect

Progress in Nuclear Energy

journal homepage: www.elsevier.com/locate/pnucene

Improvement of the European thermodynamic database NUCLEA

S. Bakardjieva [a], M. Barrachin [b], S. Bechta [c], D. Bottomley [d], L. Brissoneau [e], B. Cheynet [f], E. Fischer [f], C. Journeau [e,*], M. Kiselova [g], L. Mezentseva [h], P. Piluso [e], T. Wiss [d]

[a] Institute of Inorganic Chemistry, Czech Acad. Sci., Rez, Czech Republic
[b] Institut de Radioprotection et de Sûreté Nucléaire, BP 3, St Paul lez Durance, France
[c] Aleksandrov Research Institute of Technology, NITI, Sosnovy Bor, Russia
[d] European Commission, Joint Research Centre, Institute for Transuranium Elements, P.O. Box 2340, 76125 Karlsruhe, Germany
[e] CEA, DEN, Cadarache, F-13108 St Paul lez Durance, France
[f] Thermodata, 6 rue du Tour de l'Eau, F–38400, St Martin d'Hères, France
[g] Nuclear Research Institute UJV, Rez 250 68, Czech Republic
[h] Institute of Silicate Chemistry, Russian Acad. Sci., St Petersburg, Russia

Keywords:
Corium
Severe accidents
Thermodynamic
Database

A B S T R A C T

Modelling of corium behaviour during a severe accident requires knowledge of the phases present at equilibrium for a given corium composition, temperature and pressure. The thermodynamic database NUCLEA in combination with a Gibbs Energy minimizer is the European reference tool to achieve this goal. This database has been improved thanks to the analysis of bibliographical data and to EU-funded experiments performed within the SARNET network, PLINIUS as well as the ISTC CORPHAD and EVAN projects.

To assess the uncertainty range associated with Energy Dispersive X-ray analyses, a round-robin exercise has been launched in which a UO_2-containing corium–concrete interaction sample from VULCANO has been analyzed by three European laboratories with satisfactorily small differences.

1. Introduction

The calculation of fuel degradation, melting, melt relocation, in-vessel pool behaviour and ex-vessel spreading or interactions, as well as of fission products retention/release are based on the physical and thermochemical properties of the corium (viscosity, heat conductivity, density, solid/liquid fraction, etc.). The evaluation of these properties requires the knowledge of the *phase diagrams* of the binary, ternary and more complicated systems present in the in- and ex-vessel scenarios. Phase diagrams are directly obtained by experiments measuring phase domain limits (e.g. transition temperatures as liquidus and solidus points) or indirectly by thermodynamic measurements and models. This knowledge is a crucial aspect of the interpretation of severe accident experiments (Journeau et al., 2001; Barrachin, 2008) as well as of severe accident modelling.

Thanks to the ENTHALPY project (De Bremaecker et al., 2003), the unique European tool NUCLEA, a commonly agreed thermodynamic database for in- and ex-vessel applications, has been developed and intensively validated. Moreover, methodologies to couple the database to Severe Accident codes used by end-users have been proposed. This database (Cheynet et al., 2004; Cheynet, 2007) is continuously evolving and it takes advantage of the data acquired from bibliographical surveys and extensive experimental programs. Within the SARNET work packages on corium issues, a specific task has been dedicated to corium thermochemistry databases and in particular to the research and improvement of the NUCLEA database.

In a first section, the NUCLEA database is described. Then the comparison between thermodynamic calculations and experimental results obtained in the framework of the different projects is presented. These results arise either from specific experiments or from experiments performed within SARNET or EC-funded ISTC projects. These new data were used to improve the NUCLEA database during the 4½ years duration of the SARNET project or will serve for future improvements. Finally, since the uncertainty of the experimental results used to validate and improve the thermodynamic database varied, a round-robin exercise has been conducted in order to compare the analyses made by three different European laboratories on the same corium sample.

2. The NUCLEA database

Since 1990, severe accident experts have been interested in the assessment of thermodynamic data for a number of compounds of

* Corresponding author. Tel.: +33(0)4 42 25 41 21; fax: +33(0)4 42 25 77 88.
E-mail address: christophe.journeau@cea.fr (C. Journeau).

0149-1970/$ – see front matter © 2009 Elsevier Ltd. All rights reserved.
doi:10.1016/j.pnucene.2009.09.014

reactor materials and fission products based on the recommendations of a specialists meeting held in JRC Ispra (Nichols, 1990). Critical assessments have been made on a very large number of compounds and systems. NUCLEA is a specific Thermodynamic Database built for collecting all this knowledge.

From a general point of view, NUCLEA is a self-consistent database designed for thermochemical equilibria calculation codes and is specially developed for in- and ex-vessel nuclear applications related to LWR severe accident scenarios. It contains 18 + 2 elements: O–U–Zr–Ag–In–B–C–Fe–Cr–Ni–Ba–La–Sr–Ru–Al–Ca–Mg–Si + Ar–H and includes the following 15 oxide systems: UO_2–ZrO_2–In_2O_3–B_2O_3–FeO–Fe_2O_3–Cr_2O_3–NiO–BaO–La_2O_3–SrO–Al_2O_3–CaO–MgO–SiO_2. This database covers the entire range from metal to oxide domains. It allows the user to calculate the thermochemical equilibrium state at any step of a severe accident and to use the results to improve the predictions of core degradation codes. The database has been described by Cheynet (2007).

The binary and ternary Gibbs energy parameters were critically assessed by means of sophisticated optimization procedures. These thermodynamic parameters provide a consistent analytical description of the phase diagrams, chemical potentials, enthalpies of mixing, heat capacities, etc.

Applications of a global thermodynamic approach, i.e. the simultaneous use of a high-quality thermodynamic database and an equilibrium calculation code, are numerous:

- Condensed state phase diagrams, transitions, liquidus/solidus ranges, phase compositions and amounts,
- Coupling of thermodynamics and thermo-hydraulics,
- Calculation of viscosity, phase segregation and residual power distribution,
- Gaseous fission products release.

Such a database is much more than a compilation of thermodynamic data from various sources, its constitution needs considerable analysis for self-consistency, to ensure that all the available experimental information is satisfactorily reproduced. The condensed solutions (48 non-stoichiometric phases based on 281 reference substances) were deduced from the analysis of the assessed subsystems (binary, ternary, etc.); some of them present possible miscibility gaps. 511 condensed stoichiometric compounds were added with more than 200 gaseous species as an ideal mixture. Hydrogen was added because it is a major component of the system. Nevertheless, dissolution of hydrogen in condensed solid and liquid solutions is not taken into account up to now.

A validated thermodynamic database is characterised by a good agreement between calculated and available experimental results (phase diagrams and thermodynamic properties). This applies to tests designed for appropriate basic sub-systems or large integral experiments, made in similar conditions and at thermodynamic equilibrium. A set of 153 (18*17/2) metal–metal or metal–oxygen binary systems based on 18 pure elements and 105 (15*14/2) oxide pseudo-binary systems based on 15 pure oxides are integrated in NUCLEA. Due to the very high number of possible ternary (18*17*16/3*2 = 816) and pseudo-ternary (15*14*13/3*2 = 455) systems, it is completely unimaginable to assess all of them in the current timescale. For that reason it was decided to assess only the most important ternary systems for practical applications.

For each assessed system, the order number, source and a provisional quality criterion were given. This criterion was based on comparison between calculation and available experimental data, and has been established as follows: ✳ *Estimated* No experimental data available; ✳✳ *Perfectible;* Some domains need more experimental information (phase diagram or thermodynamic properties); ✳✳✳ *Acceptable* The system is well known and satisfactorily modelled; ✳✳✳✳ *High quality* The system is very well known and modelled. [It must be stressed that the quality criterion takes into account both phase diagram and thermodynamic properties, and thus cannot apply to parts of a phase diagram. This point is fundamental for the modelling of multicomponent systems. Moreover, it must be kept in mind that the quality criteria remain somewhere subjective, and the improvement of existing subsystems with newly available experimental results is a continuous task, which is an important part of the database management and updating.]

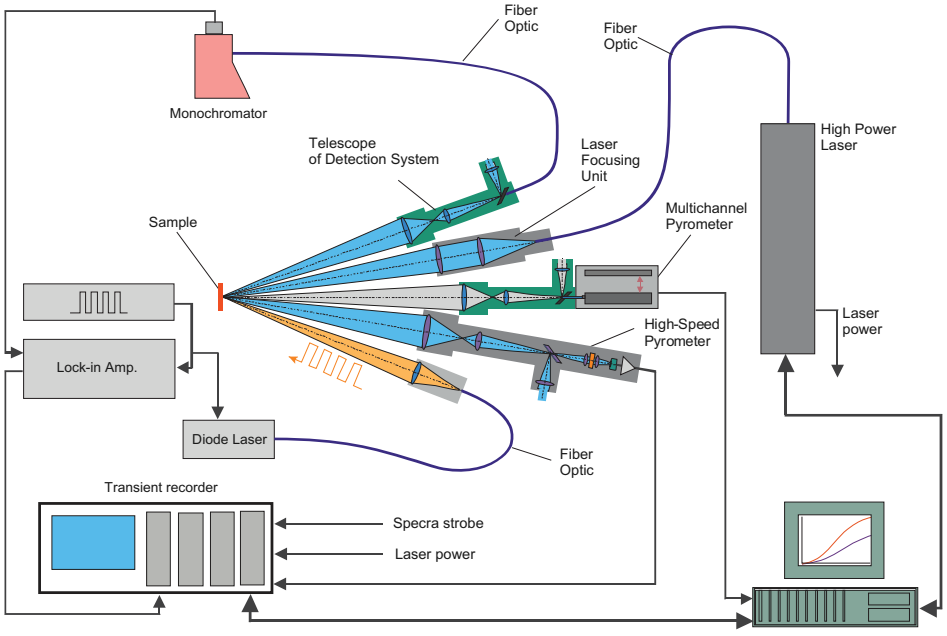

Fig. 1. Laser flash set-up for phase diagram studies at ITU.

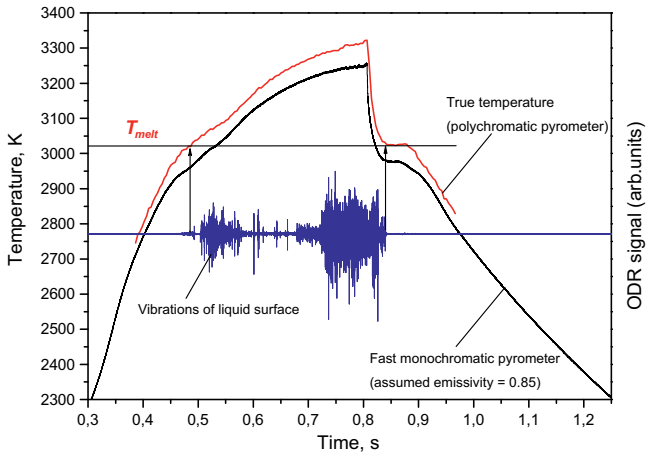

Fig. 2. Laser heating of UO_2–5 mol.% Zr.

3. Validation on experiments

3.1. Experiments at ITU

Experiments were performed at ITU to investigate the melting points (liquidus and solidus temperatures) of the U–Zr–O system by the laser flash heating technique (Fig. 1). The hypostoichiometric region of the U–Zr–O phase diagram is a key system for in-vessel melt retention. The samples were prepared from UO_2 and ZrO_2 or Zr powders by pressing into pellets and sintering under inert/lightly reducing conditions at 1700 °C (further details are given by Sheindlin et al., 2004; Manara et al., 2005). Samples were then mounted and polished for metallographic examination to verify the condition of the starting material. This revealed the metallic Zr precipitates in the UO_2 matrix were uniformly dispersed and no larger than 100 μm for a laser-heating zone of ~5 mm diameter & pyrometer-sensing zone of ~2 mm diameter in the centre of the laser-heating zone. Therefore the melt zone would include a representative sample of the material.

A second identical sample was used for melting point measurement. The power laser heats an area (~5 mm diameter) of the polished sample under pressurized inert atmosphere to beyond its melting point. The temperature of the centre of the laser-heated surface is then monitored by 2 pyrometers (a multi-channel and a rapid, 2-channel pyrometer for calibration) and from the temperature arrests during the cool-down phase, the phase transition points are determined. There is also a second laser and detector to monitor the melting of the sample surface by reflectivity changes. As an example, a melting trace for a UO_2–5 mol.% Zr is given in Fig. 2.

The liquidus and solidus temperatures experimentally determined for various compositions are indicated on the pseudo-binary UO_2–Zr phase diagram previously proposed by Juenke and White (1970) in Fig. 3 for comparison. The ITU results indicate that the liquidus temperature is rather constant below 80% mol. UO_2 on the UO_2–Zr(O) section and seems to be compatible with the presence of a miscibility gap (MG) along the UO_2–Zr(O) composition line This, in turn, supports the modelling of the U–Zr–O system in NUCLEA in the hypostoichiometric domain, based on the Juenke & White's experimental data also showing a MG on the UO_2–Zr section.

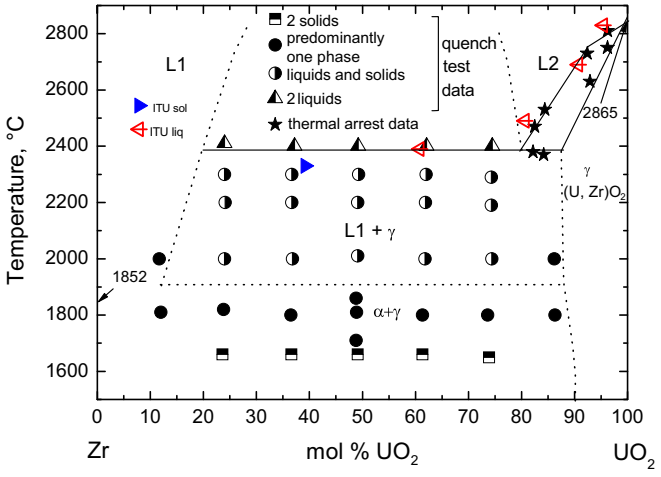

Fig. 3. Zr–UO_2 pseudo-binary phase diagram (Juenke and White, 1970) with ITU's liquidus & solidus temperatures indicated.

3.2. Experiments at UJV

Within the ECOSTAR and SARNET projects, experiments modelling corium formed under severe accidents of VVER type rector have been performed in UJV Řež (Nuclear Research Institute) using the COMETA facility with induction heating in a cold crucible. Compositions in the U–Fe–Zr–Si–O system, representative of the corium after its interaction with concrete, have been specifically investigated. Compositions of all experimental samples are shown in Table 1.

The miscibility gap phenomenon was observed during induction melting in the cold crucible in air. So the experiments with oxide mixtures were carried out with the aim to assess the extent of this phenomenon.

Experiments in cold crucible covered:

- Melting of oxide mixtures in air up to 3273 K with overheating of melt;
- Video recording of the melt surface for the appearance of the second liquid and for the behaviour of the melt;
- Computer collection of experimental data;
- Melt sampling using metallic rod (melt solidification in contact with cold metal) to/obtain quenched samples;
- Controlled melt crystallization under equilibrium conditions;

Table 1
Corium experiments performed in COMETA facility.

Experiment	Composition [wt%]					
	UO_2	Fe_2O_3 (Fe_3O_4)	ZrO_2	SiO_2	CaO	Cr_2O_3
URAN1	66	3	16		15	
URAN2	66	3	16		15	
URAN3	66	3	16		15	
URAN4	47.5	29.5	19.7			3.3
URAN5	47.5	29.5	19.7			3.3
URAN6	42.8	26.6	17.7	10		3
URAN7	56	3	14	12	15	
URAN8	50	50				
URAN9	77	3	20			
URAN10	99	1				
URAN12	56	3	14	12	15	
URAN13	64.22	2.75	13.76	5.5	13.76	
URAN14	54	3	13	15	15	
URAN15	50	50				
URAN16	43.72	29.14	27.14			
URAN17	30	50	20			
URAN18	83			17		
URAN19	50			50		

Experiments URAN 1 – 14: during ECOSTAR project; Experiments URAN 15 – 18: during SARNET project.

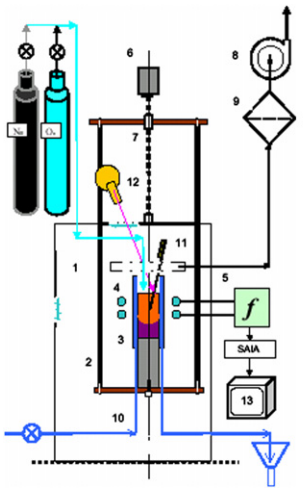

1 —melting chamber with illuminators,
2 —supporting movable frame,
3 —cold crucible,
4 —inductor,
5 —high-frequency generator,
6 —drive mechanism for moving frame (2)
7 —ball-and-screw couple of the moving mechanism,
8 —ventilator of the gas-purification system,
9 —filter
10—water-cooling system,
11—aerosol sampler,
12—radiation pyrometer or videocamera,
13—PC based information and measuring system.

Fig. 4. Scheme of the COMETA facility.

- Rapid cooling of the final melt pool, ingot cooling and removal from crucible;
- Preparation of samples for post-test analysis;
- SEM-EDS and X-ray analysis of samples;
- Construction of phase diagrams on the basis of obtained results, hypothetic diagram variants with MG areas according to experimental results;

Melting experiments were performed in UJV using the COMETA facility (Fig. 4). The equipment is adapted for the treatment of radioactive materials, especially UO_2 and thus modelling of real corium melts. A high-frequency tube generator provides 60 kW power in melt and a stable melting regime for the growth of large crystals.

The post-test analyses were carried out in UACH Řež (Institute of Inorganic Chemistry). Scanning Electron Microscopy with Energy Dispersive X-ray (SEM/EDS) analyses were carried out using scanning electron microscope SEM XL 30 Philips CP with the ROBINSON (RBS) detector. The residual pressure in the chamber of the SEM equalled 0.5 mBar, the accelerating voltage was 30 kV. For X-ray analyses PANalytical X'Pert PRO Diffractometer X' Celerator was used.

Data processing was carried out at St. Petersburg's Universities (Petrov et al., 2008). The phase diagram was constructed using calculation program DIATRIS 1.2. In Fig. 5 the calculation of the UO_2–ZrO_2–$FeO_{1.33}$ system with indicated MG areas is shown, according to different experimental data obtained in the ECOSTAR and SARNET projects. Up to now, only the results related to the investigation of the Fe_2O_3–ZrO_2 section (Petrov et al., 2004) have been taken into account in NUCLEA. The other experimental data related to the UO_2–ZrO_2–$FeO_{1.33}$ diagram and more specifically related to the different miscibility gap extensions in the ternary section is envisaged to be implemented in a coming version of the NUCLEA database.

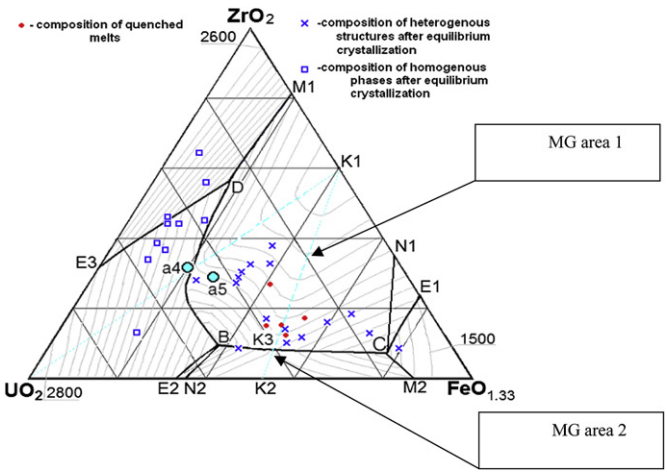

Fig. 5. Calculation diagram of system UO_2–ZrO_2–$FeO_{1.33}$ deduced from experimental data [wt%].

3.3. Experiments at CEA

3.3.1. Corium–concrete experiments

The VULCANO VB-U5 corium–concrete interaction test (Journeau et al., 2009) consisted in pouring about 28 kg of molten corium–concrete mixture of the following composition (in mass %): 54% UO_2, 38% ZrO_2, 1% CaO, 4% SiO_2, 3% Fe_3O_4 inside a concrete crucible. The concrete (Table 2) is made from CEM I 52, 5N cement and 80% siliceous aggregates from the GSM gravel pit at Rumersheim.

The overall concrete mass composition is: 63% SiO_2, 16% CaO, 9% CO_2, 5% Al_2O_3, 3% H_2O, 1.4% Fe_2O_3, 1.3% Na_2O, 1.3% K_2O.

The corium was melted in the VULCANO furnace and transferred at an initial temperature of about 2400 K into a concrete crucible. The concrete test section is surrounded by an inductor providing an average power of 25 kW to simulate decay heat. This power was maintained during 2 h 30 min and lead to 6 cm of ablation of the concrete in the radial direction and 1 cm in the axial direction.

A pseudo-binary phase diagram between corium and concrete has been calculated using GEMINI2 and the NUCLEA (version 05) database. It shows the presence of a large miscibility gap in which two liquids, one richer in silica, one poorer in silica, coexist. It must be stressed that, contrary to what occurs in binary systems, the major part of the miscibility gap lies below the liquidus, i.e. the two liquids are in equilibrium with at least one solid phase, so it is more precisely termed as multiphase monotectic equilibrium.

After the test, the corium was dismounted and some greenish glassy structures were found inside the pool (Fig. 6). SEM and EDS analyses suggest that a silico-calcareous glass was formed. In the SEM view, globules of a silica-rich liquid (L1) suspended in a urania–zirconia-rich liquid (L2) were observed, which confirms the presence of a miscibility gap in the pseudo-binary diagram.

Table 2
Concrete formulation.

Constituents	Sand 0–2 mm	Sand 0–6 mm	Gravel 5–8 mm	Gravel 8–11 mm	Gravel 11–16 mm	Cement CEM I 52, 5N	Water
Mass fraction (%)	12.2	18.4	16.6	20.4	10.4	15.3	6.7

3.3.2. Corium–concrete thermodynamic calculations

Table 3 presents typical compositions of the two liquids L1 and L2, obtained from EDS measurements of typical surfaces, and converted to oxides with the help of GEMINI2 code (Cheynet et al., 2002) and NUCLEA (Version 2005) database. Sums are not exactly equal to 100% due to the presence of non reported minor species and the oxygen non stoichiometry (not reported in this table).

Table 3
Experimental and computed compositions of the two liquids at 2200K *ACS stands for Alumina Calcium Silica compound oxides.*

%mol	SiO_2	$CaSiO_3$	ZrO_2	UO_2	ACS	Al_2O_3	FeO_x
L1 (exp.)	42	25	13	7	3	1	5
L2 (exp.)	31	19	25	15	-	2	-
Calc1 (liquid 1 of L1)	48	28	8	4	6	2	6
Calc2 (liquid 2 of L1)	31	20	23	14	2	2	6

3.3.2.1. Miscibility gap in U–Zr–Si–Ca–O system. Thermodynamic calculations have been performed using GEMINI2 and NUCLEA (version 2005) to confirm the existence of a miscibility gap and to determine the compositions of both liquids L1 and L2. The relative mole fraction of the two liquids L1 and L2 has not yet been experimentally measured. For this reason, the two liquids, L1 and L2, were considered individually to perform thermodynamic calculations.

Liquid L1 is considered first. A miscibility gap between 1500 and 2200 K and the compositions of two liquids at 2200 K were calculated (denomination Calc1 and Calc2 in Table 3). The urania–zirconia liquid (Calc2, representing 1/3 in moles of the total liquids) is close to the experimental composition of L2, whereas the silica-rich liquid (Calc1) is significantly enriched (by ~10 mol.%) in silica compared to the experimental liquid (L1) as well as having only half of its ZrO_2 content.

For the second liquid L2, the calculation gives also a miscibility gap between 1500 and 2200 K. The calculated compositions are close (within compositional uncertainties) to those found experimentally for L1. However, in this case there is 7 times more (in moles) of liquid Calc2 than of liquid Calc1.

There is today a clear need to improve our knowledge of the miscibility gap in the corium–concrete systems. Currently, according to Hudon and Baker (2002) review paper, the ($CaO–SiO_2$) miscibility gap has been well established, as have the $FeO–SiO_2$ and the $ZrO_2–SiO_2$ miscibility gaps. On the contrary, it is considered that the data on the $UO_2–SiO_2$ miscibility gap, with data only from Lungu (1966), should be considered unreliable. Experiments in the coming ISTC PRECOS project are foreseen in order to fill this gap.

Densities of both liquids L1 and L2 at 2400 K have been estimated as 3100 and 3960 kg/m^3, respectively. This density difference of 20% would be able to 'drive' the rise of L1 above L2 and cause convective movements.

Finally, during the cooling of these melts, the first solids to appear are a urania-rich face-centered cubic (FCC) phase, and a zirconia-rich tetragonal phase. The chemical compositions of these phases have been experimentally observed by SEM/EDS analyses. There is a satisfactory fit for the deposited solids, nevertheless the study will continue on this aspect for the bulk of VB-U5 corium pool.

3.3.2.2. Solubility limit of Ca in U–Zr–O phases-. The central part of the pool consisted of one liquid phase. A composition of this region is (in mol.%): 14.7% Zr, 9.8% U, 2.9% Si, 2.2% Ca, 0.5% Fe, 0.2% Mg, 0.1% Al, 69.4% O

The GEMINI2 calculation with NUCLEA (version 2005) provides a liquidus temperature of 2640 K and a solidus of 1410 K. The first solid phase to appear in the calculation is a zirconia-rich face-centered cubic phase with $U_{0.36}Zr_{0.61}Ca_{0.01}O_{2.02}$ composition. It is close to an EDS measurement of $U_{0.36}Zr_{0.56}Ca_{0.05}O_{2.21}$ (major U–Zr oxide phase). The major discrepancy between experiment and model lies with the solubility limit of calcium in $(U, Zr)O_{2+x}$, which seems much larger than the 1% calculated solubility. Such "large" solubility of CaO in zirconia–urania face-centered cubic phase was indicated by Deem (1966). It might be an effect of oxygen hyperstoichiometry.

The second phase to appear in the calculation, at 2200 K, is a second face-centered cubic solid solution with a composition of $U_{0.9}Zr_{0.1}O_{2.1}$. It is close to another experimentally measured composition: $U_{0.58}Zr_{0.13}Ca_{0.17}Si_{0.1}O_{2.17}$. If the latter is not an artefact due to the vicinity of the Si, Ca-rich matrix, then it also seems to have a larger solubility of calcium (and of silicon) in the solid solution compared to the calculated result.

Then, at 2100 K, a tetragonal phase, $Zr_{0.87}U_{0.13}O_2$ appears in the calculation, which is similar to the observed $Zr_{0.75}U_{0.18}Ca_{0.04}O_{2.11}$ phase (star-like forms of about 5 μm), which have solidified from the boundaries of the large FCC phase nodules.

3.3.2.3. U_3O_8. Some U_3O_8 (26 mol.% at 2100 K, 36 mol.% at 1500 K) was also computed but not been observed in the SEM micrographs. A possible explanation is that this is due to a partly wrong evaluation of the oxygen activity for the oxides in the U–Zr–Ca–O system or experimental errors with the oxygen estimation. A second explanation is an insufficient detectability of U_3O_8 phase: XRD

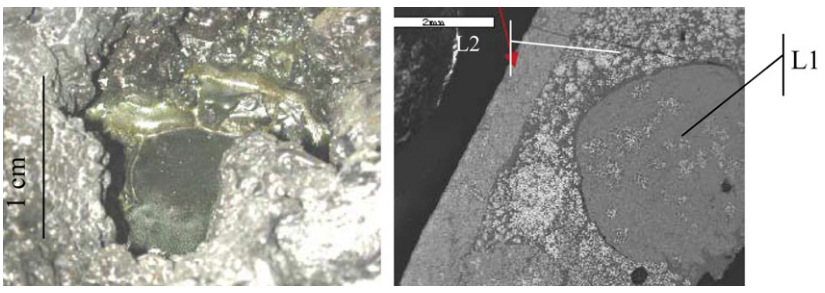

Fig. 6. One of the greenish corium vesicles left: general view – right: SEM view (sample 13_1 zone B) showing two liquid phases, L1 and L2.

analyses provide information on the effective presence of U_3O_8 in the corium sample only if there are at least 2% vol. of this phase present.

At this stage, most of the refractory materials is in the form of a mixed oxide with an U/Zr ratio close to the NUCLEA calculations performed assuming a (Scheil, 1942; Gulliver, 1922) solidification path (infinite diffusion in liquids, no diffusion in solids) which supports the fact that the cooling during the VB-U5 test was far from equilibrium.

In conclusion, the GEMINI2 calculations with NUCLEA (version 2005) provide useful information on the solidification of the VB-U5 central pool.

3.4. Experiments at NITI (CORPHAD–PRECOS)

In 2003, NITI and ISC RAS implemented the ISTC CORPHAD (Corium phase diagrams) project funded by the European Commission. One of CORPHAD's objectives was to investigate phase equilibria in the following binary and ternary systems: ZrO_2–FeO, UO_2–FeO, FeO_x–SiO_2, and U–O, U–Zr–O, Fe–Zr–O, U–Fe–O which depend on oxygen partial pressure. The CORPHAD data on ternary systems are especially relevant for the phase equilibrium investigation in the miscibility gap domain of the U–Zr–Fe(Cr, Ni, Mn)–O system which is of particular interest for corium in-vessel retention. The phase diagram study of several systems, particularly UO_2–SiO_2 and U–Zr–Fe–O, has been continued in the frame of the recently started ISTC PRECOS (Phase relations in corium systems) project also funded by EU. Some of the CORPHAD results are listed hereunder.

3.4.1. ZrO_2–FeO and UO_2–FeO systems

The data on the ZrO_2–FeO_{1+x} and UO_2–FeO_{1+x} systems studied in a neutral atmosphere are presented as phase diagrams in Figs. 7 and 8. The detailed results can be found in Bechta et al. (2006, 2007a). The most important results are:

- The refined eutectic point in the first system (ZrO_2–FeO_{1+x}) was found to correspond to a ZrO_2 concentration of 10.3 ± 0.6 mol.% at 1605 ± 5 K. The solubility limit of iron oxide in zirconia was determined in a broad temperature range, taking into account the ZrO_2 polymorphism.
- The eutectic point in the second system (UO_2–FeO_{1+x}) corresponds to a temperature of 1608 ± 5 K and a UO_2 concentration of 4.0 ± 0.1 mol.%. The maximum solubility of FeO in UO_2 at the eutectic temperature was estimated as 17.0 ± 1.0 mol.%.

Optimization of these binary oxidic diagrams in NUCLEA by taking into account these new results (Figs. 7 and 8, a vs. b) enables more complex systems representing oxidized corium to be modelled in more details. Details of the modifications of the NUCLEA modelling are given thereafter (see section NUCLEA improvements).

3.4.2. FeO_x–SiO_2 systems

The influence oxygen partial pressure on the phase equilibrium in SiO_2–Fe_2O_3(Fe_3O_4) systems of has been studied by Mezentseva et al. (2006) in CORPHAD. At lower oxygen partial pressure ($p_{O_2} = 0.1$Pa) the system belongs to the SiO_2–Fe_3O_4 polythermal section. With increasing p_{O_2} from 0.1 to 1.0×10^5 Pa the quasi-binary SiO_2–Fe_3O_4 and SiO_2–Fe_2O_3 systems belongs to the SiO_2–Fe_3O_4–Fe_2O_3 concentration triangle due to FeO_x stoichiometry. Up to now, there were practically no experimental data for the SiO_2–Fe_2O_3(Fe_3O_4) systems. Two hypothetical models of the SiO_2–Fe_2O_3 section were available, one from AEA-T (Mignanelli, 2003) and the other one from Selleby (1997). The monotectic temperature in particular differed between both versions since the former version indicated 1940 K and the latter one 1863 K. It was experimentally shown in CORPHAD, that all SiO_2–Fe_2O_3(Fe_3O_4) systems contain a miscibility gap region at temperatures higher than 1818 ± 11 K (average value for the three systems); the contents of the coexisting phases depend on oxygen partial pressure. The CORPHAD results obtained on the SiO_2–Fe_2O_3 section (in air) show a rather good agreement with Selleby's calculated section.

All the transformations are illustrated by Fig. 9. The scheme proves that changing oxygen partial pressure over the condensed phases of the SiO_2–Fe_2O_3(Fe_3O_4) system equally affects the character and temperature of the phase and chemical transformations. The oxygen partial pressure above all governs the combination of the iron oxides that exists under certain p_{O_2}. All these experimental results were used to improve the modelling of the Fe–O–Si system in NUCLEA.

3.4.3. U–O system

Fig. 10 shows the comparison of the CORPHAD data on the U–O system obtained under inert atmosphere with results of other authors. Discrepancies in the experimental values of the oxygen solubility in the uranium melt at high temperature and in the extent of the miscibility gap (MG) clearly appear in the figure. In accordance with Edwards and Martin (1966), the wide MG with two liquids (L_1 and L_2) lies in the domain between 0.05 and 0.60 atomic fractions of oxygen, while, in accordance with Guinet et al. (1966) the MG is very small – between 0.52 and 0.58 atomic fractions of O at 2773 K.

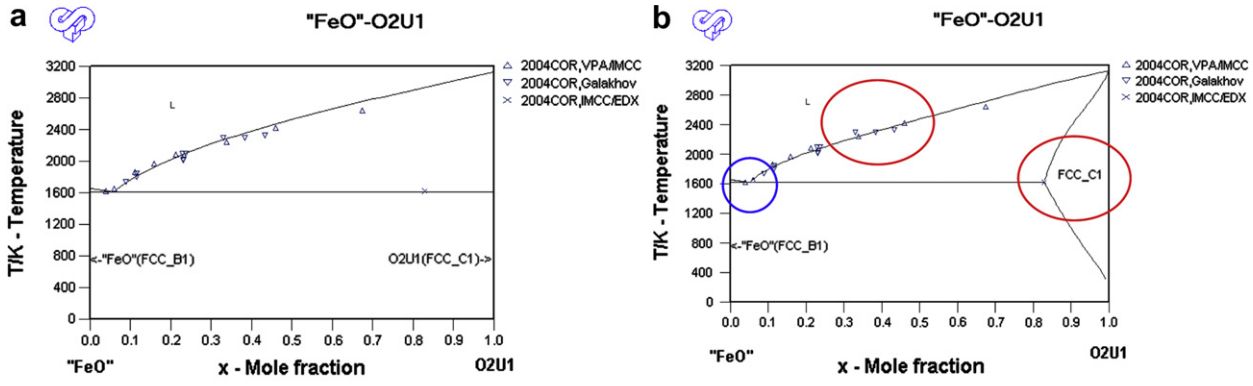

Version 2004 of phase diagram with CORPHAD data points added

Version optimized with main modifications due to CORPHAD data

Fig. 7. NUCLEA representation of UO_2–FeO_{1+x} phase diagram.

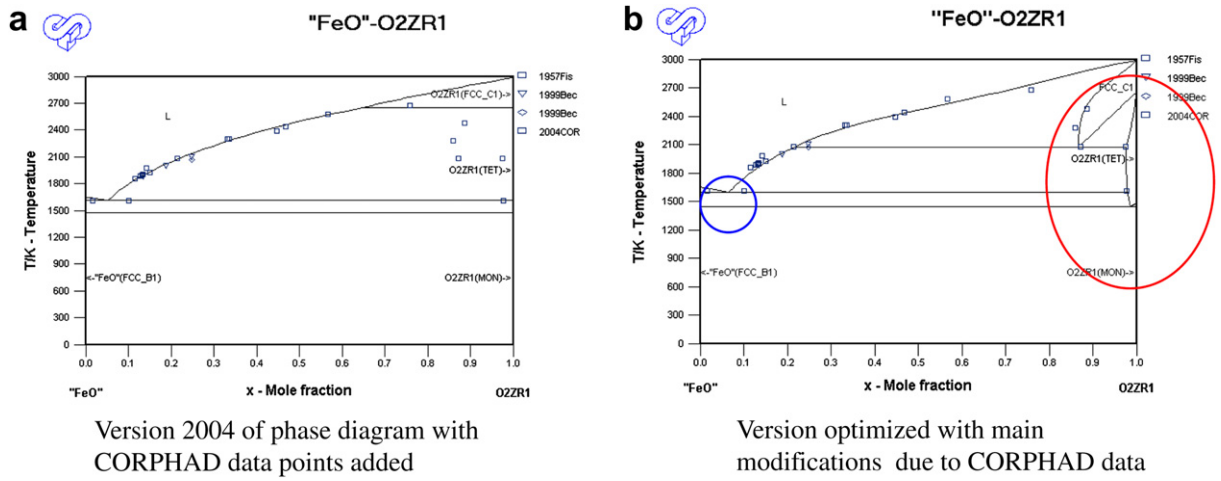

Version 2004 of phase diagram with CORPHAD data points added

Version optimized with main modifications due to CORPHAD data

Fig. 8. NUCLEA representation of ZrO_2–FeO_{1+x} phase diagram.

The CORPHAD results are in quantitative agreement with the data of the more recent experiments of Guéneau et al. (1998) obtained at high temperature. These results confirm the presence of a wide miscibility gap (MG) in this system. In CORPHAD, the measured extension of the MG is only slightly smaller than the values of Guéneau et al. (1998) values. At 2950 K, the oxygen solubility in metallic uranium is about 2 at. % higher than the solubility indicated by Guéneau et al. (1998) at 3090 K (Fig. 10).

However, the melt temperature in Guéneau et al. (1999) test was not measured directly, but was calculated from evaporation data with a resulting uncertainty of ±100 K. Therefore the reason for the difference in oxygen solubility could be associated either with the difference in temperature or with a methodological error in calculating temperature. Considerable error bars for the oxygen solubility in metal in CORPHAD (Fig. 10) should be pointed out here.

3.4.4. U–Zr–O system

Hypostoichiometric regions of the U–Zr–O phase diagram are known to exhibit a MG between two liquids of the compositions $(U,Zr)O_{2-x}$ and U–Zr–(O). The orientation of the tie-lines in this two-phase domain was measured by Guéneau et al. (1998) at very high temperature 3090 K. A large number of compositions was investigated in CORPHAD at lower temperatures (2600–2800 K, Fig. 11, right). The lower temperatures are of interest since they are closer to the temperatures reached in the MASCA test (Asmolov and Tsurikov, 2004). Among the different tests, a MG was registered only for three compositions (Fig. 11, right).

Among the different investigated compositions, a MG was registered only for three compositions indexed 41, 42 and 37 on Fig. 11, right at 2573 K. For compositions 42 and 37, the experimental observation of a MG is consistent with the NUCLEA modelling (Fig. 11 left). In contrast, for composition 34 located on the UO_2–Zr section, separation between two liquids at 2573 K is foreseen by NUCLEA (Fig. 11 left). It must be noticed that NUCLEA slightly underestimates the temperature of MG appearance in comparison with the past experimental data (Fig. 3) of Juenke and White (1970) on which the NUCLEA modelling of the U–O–Zr phase diagram is based. Indeed these authors noted the liquid separation above 2623 K, which is consistent with the absence of MG registered in the CORPHAD test performed only at 2573 K. For other compositions located in the triangle UO_2–ZrO_2–Zr, in particular on the section UO_2–αZr(O), there is no indication of MG, which is in

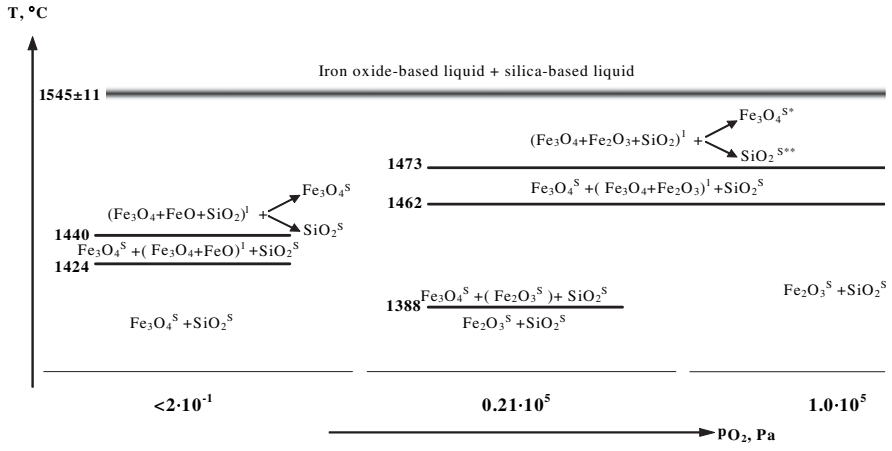

. *In the region of primary crystallization of Fe_3O_4

**In the region of primary crystallization of SiO_2

Fig. 9. Schematics of the phase and chemical transformations in the SiO_2–Fe_2O_3(Fe_3O_4) system at various oxygen partial pressures according to Mezentseva et al. (2006).

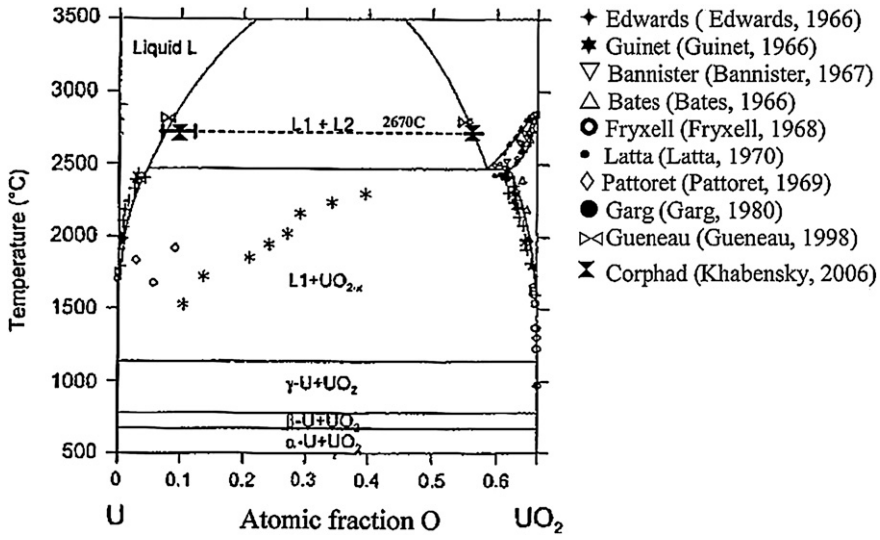

Fig. 10. Phase diagram of the U–O system with the different existing data.

agreement with experimental data of Hayward and George (1996) and with the NUCLEA modelling.

For two of these compositions (namely 42 and 37, Fig. 11, right), for which the compositions of the phases at equilibrium were experimentally determined, thermodynamic calculations using the GEMINI2 code and the NUCLEA database were performed for comparison (Table 4). The modelling of the U–Zr–O subsystem in this database takes into account the experimental data of Guinet et al. (1966) on the U–O and U–Zr–O systems at high temperature (>3000 K) and allows the U–Zr–O phase diagram to be presented at lower temperatures (Fig. 11, left, 2573 K, see Chevalier et al. (2004) for the complete modelling). It then makes possible the comparison between the CORPHAD experimental results and the data of Guéneau et al. (1998) although they were not obtained in the same temperature range.

Experimental results of CORPHAD have only a qualitative agreement with the thermodynamic modelling of NUCLEA. The quantitative data on equilibrium compositions of liquids in the miscibility gap differ from the thermodynamic forecast, in particular for the oxygen and zirconium contents in metallic melts. The oxygen solubility in the uranium–zirconium alloys is the key point since it is tightly linked to the extension of the MG in the ternary system. Normally, the higher is the solubility, the smaller is the miscibility gap. The CORPHAD result on the U–O phase diagram (previous section) seems to confirm that the oxygen solubility in uranium–zirconium melts is limited and is in agreement with previous experimental results from Guéneau et al. (1998). From this data, it is expected to have a large MG in the U–O–Zr phase diagram in agreement with the experimental data of Guéneau et al. (1998) on U–O–Zr. The NUCLEA modelling of the U–O–Zr phase diagram is built on this assumption. The high solubility of oxygen in the uranium–zirconium alloys determined in CORPHAD tests (Table 4) indicates on the contrary that the miscibility gap is rather small and in particular does not cross the UO_2–Zr composition line in contradiction with the UO_2–Zr vertical section proposed by Juenke and White (1970). The high oxygen solubility measured in the "metallic liquid" during CORPHAD tests could be due to a partial redistribution of species during the quenching process. This internal disagreement between the different CORPHAD results (large solubility of oxygen in ternary phase diagram and small oxygen solubility in the binary U–O phase diagram) remains to be solved. The above-mentioned differences in experimental data

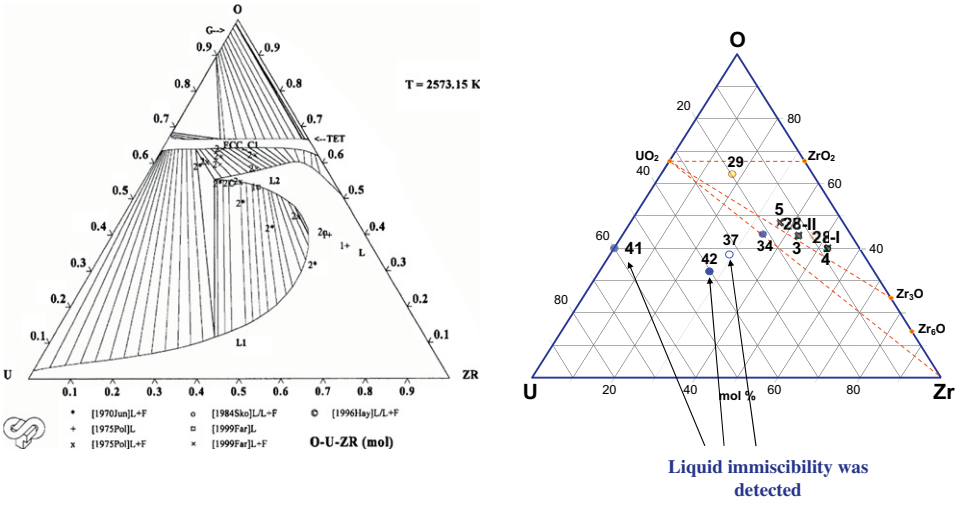

Fig. 11. Modelling of U–Zr–O system in NUCLEA2006 with the different existing data (left) and compositions tested in the CORPHAD project (right).

Table 4
Experimental data and thermodynamic calculation (GEMINI2 + NUCLEA06) of coexisting liquid compositions in the U–Zr–O system.

Composition, atomic fraction/temperature, K	Composition of metallic liquid, at%						Composition of oxidic liquid, at%					
	Experiment			Calculation			Experiment			Calculation		
	U	Zr	O	U	Zr	O	U	Zr	O	U	Zr	O
$U_{0.325}Zr_{0.292}O_{0.383}$/2643	40.8	32.2	27.0	44.0	41.5	14.5	25.1	26.7	48.2	24.8	21.1	54.1
$U_{0.405}Zr_{0.270}O_{0.325}$/2753	53.1	29.3	17.6	49.8	36.8	13.4	27.6	23.2	49.2	30.3	16.2	53.5

along with the lack of clear understanding of their physical reasons provide the motivation for continued study in the PRECOS project, which is expected to optimize the NUCLEA predictions for this system.

3.4.5. Fe–O–Zr system

There are practically no published data on phase equilibria in the high-temperature domain of the Fe–O–Zr system at low oxygen concentrations. Several experiments were conducted in CORPHAD to fill this lack. For two of these experiments, liquid immiscibility was observed. Table 5 gives the comparison of compositions provided by experiments and corresponding thermodynamic calculations using GEMINI2–NUCLEA. The CORPHAD experiments in this system showed a larger solubility of oxygen with less iron in the metallic, but more iron in the oxidic liquid compared to calculations. To be implemented in the NUCLEA database, these experimental results, in particular the absence of species redistribution between the different phases, potentially observed in the U–Zr–O tests (see previous section) during the quenching process has to be checked.

3.4.6. Fe–O–U–(Zr) system

Only one composition in the MG of the Fe–O–U system was studied within the CORPHAD project. It should be mentioned that in accordance with the post-test analysis the metallic uranium used for producing the melt in this experiment was found to have a low Zr content of 2.7 wt.%. It means that these experimental results deal with the Fe–O–U–Zr system in the region of small Zr concentration. It is known that molten steel has a very low solubility in liquid UO_2 (Spino and Schulz, 1981; Kleykamp, 1997) In this experiment it was slightly higher, which is likely to be due to the influence of zirconium.

Table 6 gives the comparison of experimental and calculated data on the composition of liquids in the MG. In contrast to the calculations, experimental data showed a larger solubility of oxygen in the metallic liquid and iron in the oxidic liquid. This is consistent with the results of the Fe–O–Zr system.

3.5. Experiments at CEA and NITI on aerosol release from molten pools

The NUCLEA database is also applicable for modelling of fission product (FP) release from molten corium. Therefore experimental information of tests with corium and fission products can be potentially used for optimization of the database.

The COLIMA CA-U3 test (Journeau et al., 2007) was performed within the PLINIUS project. A molten pool, representative of a VVER severe accident, was produced in a hot tungsten crucible with induction coils around it. The gas chosen for the test was helium with 2% hydrogen at a gauge pressure of 3 bar.

The COLIMA CA-U3 corium load (Fig. 12) is made of about 2 kg depleted uranium dioxide pellets, and powders for the other oxides (to represent oxidized cladding, steel and fission products).

The test sequence can basically be divided into three different phases: a heating-up phase, a heating plateau phase and a fission product release phase. After the heating-up phase, a long high-temperature plateau is maintained in order to achieve aerosol sampling. A corium melt temperature of 3030 K is reached and kept for more than 50 min. The test ends with crucible wall melt-through and a large flow of the liquid corium outside the crucible.

Even if the test terminated due to a crucible melt-through, the corium that stayed in the crucible was analyzed. First of all, it is estimated that the equivalent of 25 pellets did not melt. The EDS (Energy Dispersion Spectrometry) analysis shows two distinct phases in the melted corium: one main phase, 95% in volume, enriched in uranium, and, one minor phase, 5% in volume, depleted in uranium. The aerosols collected in a thermal gradient tube, filters and impactors were also analyzed.

A thermodynamic modelling of the release has been made with GEMINI2 with the NUCLEA database (version 2005). Post-test calculations are reported in Fig. 13 for two cases considering that the pool was in contact with 5% of the gas flow (fraction estimated by CFD calculations before the test) or with all the gas flow, for equilibrium calculations at 3033 K. Most of the strontium was released from the melt – contrary to the assessment value of 10% cited by Baichi (2001). This release must have occurred during the last phase of the test. Very small aerosols (geometric diameter around 0.3 μm) had been collected in the impactor. The discrepancy between this high release rate and the lower rate observed during the Phébus FPT1 test (Dubourg et al., 2005) suggests the role of molybdates (Mo was absent in CA-U3 in order to avoid interaction with tungsten) in stabilizing strontium oxides. Except for strontium, all the tendencies for the elements in the database (Ag represents Te, La represents all the lanthanides) are satisfactorily fitted. It was verified the effect of pool temperature uncertainties do not modify the calculation results qualitatively. For steel components (Fe, Cr), the high release rates seem to indicate that, assuming correct modelling, most of the gas flow was in thermodynamic equilibrium with the corium pool.

Table 5
Experimental data and (GEMINI2 + NUCLEA06) thermodynamic modelling of coexisting liquid compositions in the Fe–O–Zr system.

Composition, atomic fraction/temperature, K	Composition of metallic liquid, at%						Composition of oxidic liquid, at%					
	Experiment			Calculation			Experiment			Calculation		
	Zr	Fe	O	Zr	Fe	O	Zr	Fe	O	Zr	Fe	O
$Zr_{0.505}Fe_{0.198}O_{0.297}$/2693	53.5	23.1	23.3	51.8	31.3	16.9	No data			48.5	2.7	48.8
$Zr_{0.464}Fe_{0.253}O_{0.283}$/2773	48.7	26.1	25.2	47.2	40.2	12.7	44.8	6.4	48.8	45.3	1.7	53.0

Table 6
Experimental data and thermodynamic modelling of coexisting liquid compositions in the Fe–O–U–Zr system.

Composition, atomic fraction/ temperature, K	Element	Composition of liquids, at%			
		Experiment		Calculation	
		Oxidic	Metallic	Oxidic	Metallic
$U_{0.600}Fe_{0.216}Zr_{0.400}O_{0.144}$ 2873	U	41.0	64.0	40.0	65.6
	Fe	2.0	23.5	0.0	27.5
	Zr	2.3	3.9	1.3	4.8
	O	54.8	8.5	58.7	2.0

Tests on low volatile FP release from molten corium pool having different oxidation indexes were recently carried out by NITI in the frame of the EVAN ISTC project. GEMINI2 and NUCLEA (version 2007) were applied by Bechta et al. (2007b) both for modelling of final melt composition and FP volatilization.

With respect to the final oxidized composition, NUCLEA calculations indicate a single liquid in the pool at temperatures above liquidus (Fig. 14, left); while the dense metallic inclusion containing 88.8 mass % of Ru; 11.0% of Mo, 0.2% of Zr together with the shape and the location of this inclusion (Fig. 14, right) give evidence of liquid immiscibility.

Concerning volatilization modelling, the most complicated point for calculation of FP release with a thermodynamic code is to determine the volume of gas in local thermodynamic equilibrium with the melt. Detailed calculation of gas flows above the melt can be used for this. The volume was assessed by Bechta et al. (2007b) using the data obtained during the melt oxidation stages of the test. It these stages, an Ar/O_2 mixture was blown through the furnace with the same flow rate as Ar during FP evaporation stages. It was assumed that oxygen was completely absorbed from that part of the gas, which was in equilibrium with the melt (40% of the gas volume).

Modelling results of the 1st regime (evaporation of C-70 corium melt in neutral atmosphere, 2863 K) of EVAN-FP1 test are compared with experimental data in Fig. 15. Ce and Mo were excluded from calculations due to their absence in the used database. Fig. 15 shows that:

- The release of uranium, zirconium and barium during melt evaporation is correctly modelled by NUCLEA 2007;
- The calculated values of lanthanum evaporation in an inert atmosphere are overestimated by a factor of four;
- The releases of strontium and ruthenium are significantly underestimated.

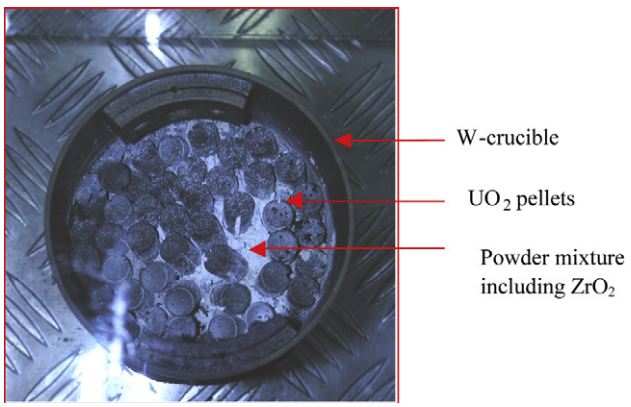

Fig. 12. Initial COLIMA CA-U3 load in the crucible.

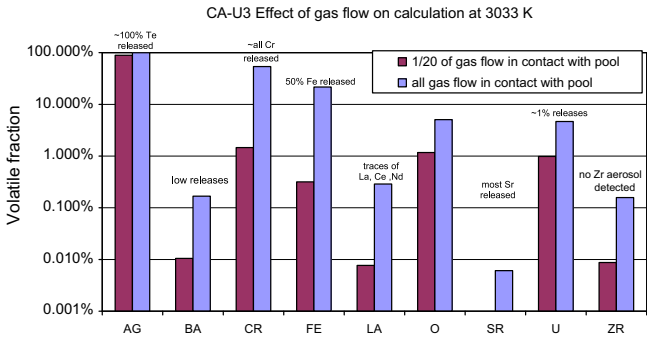

Fig. 13. GEMINI2 post-test calculations of COLIMA CA-U3.

As for the CA-U3 test (in reducing atmosphere), the release of strontium is found to be significantly underestimated.

The reasons of the listed differences for Sr and Ru release, which are important for calculation of radiological consequences, are likely to be associated with complex chemistry of these elements and problem of their modelling. Forthcoming experiments of EVAN project 2nd phase will provide more information on the specific element evaporation rates for NUCLEA database optimization.

4. Improvements of the database

Among the different "perfectible" phase diagrams, the systems including iron oxide had to be improved taking into account their impact on the thermodynamic properties of in-vessel and ex-vessel corium.

The modelling of the "FeO"–ZrO_2 pseudo-binary system has been improved by taking into account new experimental results obtained during the ISTC CORPHAD Project. Until then, this system had not been investigated in the whole composition range in the open literature. The first experimental results were obtained by Fischer and Hoffman (1957) in the FeO-rich domain, and the eutectic composition was estimated from an extrapolation method. The eutectic temperature was determined as 1603 K and the eutectic composition extrapolated as 1.7 mol.% ZrO_2. More recently new liquidus determinations (crust and thermocouple method) were performed through the CIT (Corium Interactions and Thermochemistry) European project, by Hellmann and Nie (1998), but not selected in the assessment work due to the lack of documentation. New measurements of liquidus temperatures over the whole composition domain and the accurate determination of the eutectic temperature have been performed in the CORPHAD project (see Section 3.4). The eutectic point has been found to correspond to a ZrO_2 concentration of 10.3 ± 0.6 mol.% at 1605 ± 5 K. These results allowed the refinement of the thermodynamic modelling, in both the FeO-rich domain, and also in the unknown high temperature, ZrO_2-rich domain. The new experimental data related to liquidus temperatures globally confirms the validity of the previous modelling. The most apparent evolution is the modelling of a limited solubility of iron oxide in the cubic ZrO_2-rich solid solution which might be important in calculations of multi-component systems including the Fe–O–Zr ternary system.

The FeO–UO_2 pseudo-binary system has been also re-assessed by taking into account the experimental results obtained within the framework of the ISTC CORPHAD Project. This system was, up to now, not available in the open literature. Experimental data were only obtained by Hellmann and Nie (1998) and gave an approximate eutectic temperature and composition. The new liquidus values and the determination of the eutectic temperature and composition obtained in the CORPHAD project have confirmed the

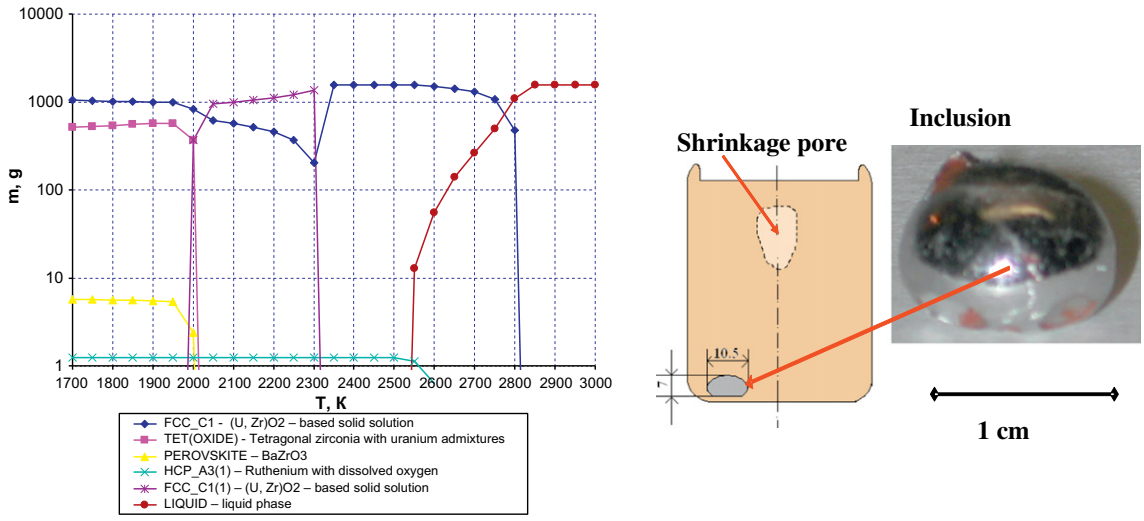

Fig. 14. Temperature evolution of phases determined by thermodynamic modelling of EVAN-FP1 final composition (left) and macrostructure of corium ingot (right).

phase diagram shape in the FeO-rich domain. The eutectic point corresponds to a temperature of 1608 ± 5 K and a UO_2 concentration of 4.0 ± 0.1 mol.%. The new experimental data were also used to refine the liquidus in the UO_2-rich domain (Fig. 7). A significant modification is finally the modelling of a limited solubility of iron oxide in the UO_2 solid solution.

The U–O phase diagram has been recently investigated at high temperature in the hyperstoichmoetric region. Up to now, the only existing experimental data at high temperature (>2500 K) were solidus and liquidus temperatures over the composition range from UO_2 to $UO_{2.23}$ measured by Latta and Fryxell (1970). These results were suspected of crucible contamination by the authors themselves. The uncertainty on the real liquidus shape in the hyper-stoichiometric field led to obtain various temperatures in the literature for the invariant reaction $L \Leftrightarrow G + UO_{2+x}$ for 1 atm total pressure: 3077 K (Chevalier et al., 2004); 2700 K (Guéneau et al., 2002); 2873 K (Levinskii, 1974). For this reason the melting of stoichiometric and hyper-stoichiometric uranium dioxide was recently thoroughly investigated by means of advanced techniques by Manara et al. (2005; see also Section 3.1). These new results allow the modelling of the O–U phase diagram in the hyper-stoichiometric field to be re-visited (Fig. 16). The monotectic reaction $L \Leftrightarrow G + UO_{2+x}$ is now calculated at 2694 K, instead of previous 3077 K.

5. Round-robin exercise

Corium is a complex multiphase material containing heavy (U) and light elements (Ca, Si as well as O), which renders its chemical analysis complex. As few laboratories are able to work with prototypic corium (containing depleted or natural uranium) and reliable results are needed to validate the thermodynamic database, it was decided to perform a round-robin exercise (Bakardjieva et al., submitted for publication) between three different European laboratories (CEA Cadarache, ITU Karlsruhe, UACH Řež) for SEM-EDS analysis of a sample (Fig. 17) from the VULCANO VB-U6 Molten Core Concrete Interaction test (Journeau et al., 2009). The purpose of the round robin is not to compare intrinsic performances of the different apparatus but rather to assess the reliability of the experimental chemical compositions and to give confidence bounds to the users of the data.

During the round robin, window average compositions were determined as well as local measurements of the compositions of the various observed phases were made. In all the measured windows, the compositions lie on the line connecting the initial corium melt composition to the average concrete composition, showing the absence of chemical segregation during the interaction process. Nevertheless, distinct zones with different concentrations in corium have been found. In terms of microstructures,

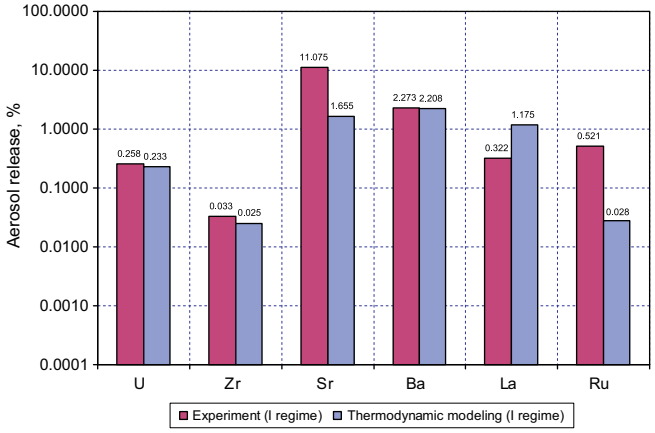

Fig. 15. Comparison of data on aerosol release thermodynamic modelling with experimental results of the 1st test regime.

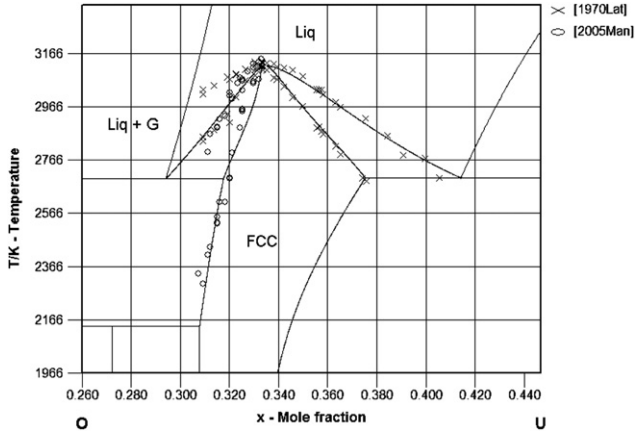

Fig. 16. Calculated phase diagram (fixed condition of $P_{tot} = 1$ atm) of the O–U binary system with new optimized parameters in the hyper-stoichiometric UO_{2+x} field.

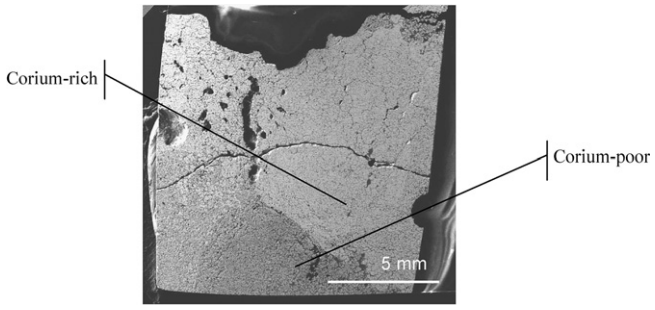

Fig. 17. Macrograph of the round-robin sample, presenting two characteristic zones.

two major phases have been found, i.e. corium-rich nodules within a concrete-rich matrix. Their relative proportions differ within the zones.

The round-robin exercise confirmed that SEM and EDS analysis can be used confidently to perform fast and good quality corium analyses and provide quantitative compositions in the metallic elements of corium with an uncertainty of 1/10th of the measured value. As an example the plot of the concentration of uranium (tracer of the corium) against that of silicon (tracer of the concrete) is given in Fig. 18 upper graph. Concerning the oxygen content (Fig. 18 lower graph), CEA and ITU results were well aligned while UACH values were 1/4th lower. In the absence of further analyses, we can only conclude that the uncertainty is clearly not random but is rather similar to a bias – possibly related to the measurement system differences between instruments. Nevertheless it is seen that the EDS analyses can provide reliable information on the relative amounts of oxygen between two phases or areas. This result supports the quality and the acceptable uncertainty range that is necessary for the (sub) systems requiring high quality criteria in the NUCLEA database.

Nevertheless, as all the analyses are currently made without calibration with respect to a "corium" standard, further work will involve the synthesis and characterization of (U, Zr)O_2 standards and also the use of alternative techniques such as wavelength dispersive analysis or microprobe analysis to try to resolve the observed differences in EDS oxygen measurements.

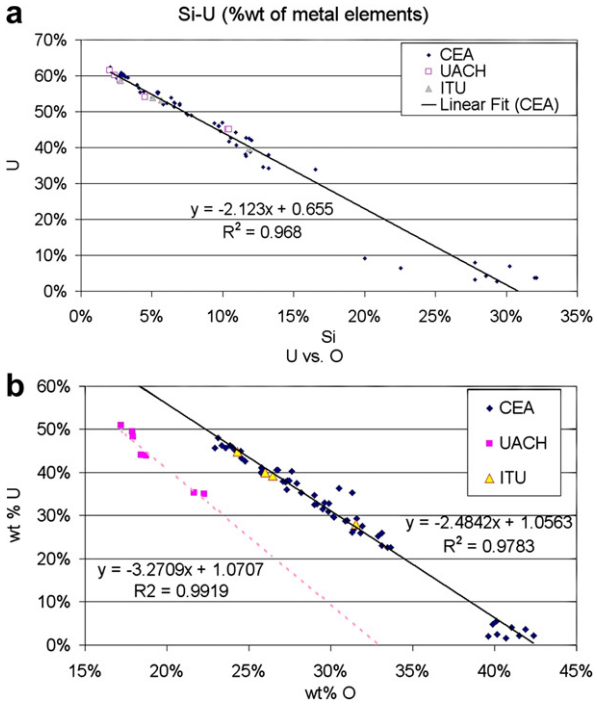

Fig. 18. Window composition correlations obtained from the three participating laboratories: (above) U vs. Si – (below) U vs. O.

6. Conclusions

Thanks to the works and efforts of the SARNET partners and of related ISTC projects, a large amount of new data relative to the corium phase diagrams has been acquired. The data represent the main subsystems of the NUCLEA database (subsystems of the U–Zr–Fe–Si–O quinary system) as well as validations of more global experiments dealing with corium–concrete interaction or molten pool fission product releases.

Quantitative corium material analyses are the necessary link between the experiment and the data needed to improve a thermodynamic database. The results of the corium SEM-EDS analyses have shown, thanks to a round-robin exercise on a corium sample, their quality and reliability. These results have served to the continuing improvement of the European reference thermodynamic database for LWR severe accidents, NUCLEA. Further improvements are still necessary, in particular regarding phase diagrams of U–Zr–Fe–O system at low oxygen potential (including more simple subsystems, such as Zr–Fe–O and U–Fe–O), the modelling of FP evaporation (particularly strontium) and the modelling of the corium–concrete interactions (including phase diagrams for ex-vessel corium). This aim will be pursued within the proposed SARNET2 project, as well as in ISTC projects in the coming years.

Acknowledgements

Most of the work presented in this paper has been part of the SARNET joint program of activities (contract SARNET FI6O-CT-2004-509065 of the EURATOM 6th Framework programme). The ECOSTAR and PLINIUS Projects were co-funded by the European Commission within the EURATOM 5th Framework Programme.

The CORPHAD, PRECOS and EVAN projects are funded by the European Commission through the International Scientific and Technical Centre.

The round-robin exercise was partly supported in 2006–2007 by the French–Czech *Barrande* project n°10783UH and the French Foreign Ministry ECO-NET project, No. 18555VE in 2008.

References

Asmolov, V., Tsurikov, D., 2004. MASCA Project: Main Activities and Results. OECD/NEA MASCA Seminar, Aix en Provence, France, June 10–11.

Baichi, M., 2001. Contribution à l'étude du corium d'un réacteur nucléaire accidenté: aspects puissance résiduelle et thermodynamique des systèmes U–UO2 et UO2–ZrO2, PhD Thesis, INPG Grenoble.

Bakardjieva, S., Bottomley, D., Brissonneau, L., Journeau, C., Kiselova, M., Piluso, P., Thiele, H., Wiss, T., Prototypic corium analysis: a round robin for SEM and EDS characterization. Material Characterization, Submitted for publication.

Barrachin, M., 2008. FPT0 and FPT1 PHEBUS Tests: Post-mortem Examination Interpretation. ANS 2008 Annual Mtg., Anaheim (CA, USA), 8–12 June.

Bechta, S.V., Krushinov, E.V., Almjashev, V.I., Vitol, S.A., Mezentseva, L.P., Petrov, Yu.B., Lopukh, D.B., Khabensky, V.B., Barrachin, M., Hellmann, S., Froment, K., Fischer, M., Tromm, W., Bottomley, D., Defoort, F., Gusarov, V.V., 2006. Phase diagram of the ZrO_2–FeO system. J. Nucl. Mater. 348, 114–121.

Bechta, S.V., Krushinov, E.V., Almjashev, V.I., Vitol, S.A., Mezentseva, L.P., Petrov, Yu.B., Lopukh, D.B., Khabensky, V.B., Barrachin, M., Hellmann, S., Froment, K., Fischer, M., Tromm, W., Bottomley, D., Defoort, F., Gusarov, V.V., 2007a. Phase diagram of the UO_2–FeO_{1+x} system. J. Nucl. Mater. 362, 46–52.

Bechta, S., et al., 2007b. Ex-vessel Source Term Analysis. Task 2 Final Report. ISTC Project # 3345 (EVAN). Alexandrov Research Institute of Technology (NITI).

Chevalier, P.Y., Fischer, E., Cheynet, B., 2004. Progress in the thermodynamic modelling of the O–U–Zr ternary system. Calphad 28, 15–40.

Cheynet, B., 2007. Nuclea. http://hal.archives-ouvertes.fr/hal-00165418/fr/.

Cheynet, B., et al., 2002. Thermosuite. Calphad 26 (2), 167.

Cheynet, B., Chaud, P., Chevalier, P.Y., Fischer, E., Masson, P., Mignanelli, M., 2004. NUCLEA propriétés dynamiques et équilibres de phases dans les systèmes d'intérêt nucléaire. J. Physique IV 113, 61–64.

De Bremaecker, A., Barrachin, M., Jacq, F., Defoort, F., Mignanelli, M., Chevalier, P.Y., Cheynet, B., Hellmann, S., Funke, F., Journeau, C., Piluso, P., Marguet, S., Hózer, Z., Vrtilkova, V., Belovsky, L., Sannen, L., Verwerft, M., Duvigneaud, P.-H., Mwamba, K., Bouchama, H., Ronneau, C., 2003. European Thermodynamical Database for In and Ex-Vessel Applications. FISA, Luxembourg (Luxembourg). 10–13 November.

Deem, H.W., 1966. Fabrication, Characterization, and Thermal-Property Measurements of ZrO2-base Fuels, Technical Report no BMI-1775, Special UC-25.

Dubourg, R., Faure-Geors, H., Nicaise, G., Barrachin, M., 2005. Fission product release in the first two PHEBUS tests FPT0 and FPT1. Nucl. Eng. Des. 235, 2183–2208.

Edwards, R.K., Martin, A.E., 1966. Phase Relation in the Uranium–Uranium Dioxide System at High Temperature, V. 2. Thermodynamics. IAEA, Vienna, p. 423.

Fischer, W.A., Hoffmann, H., 1957. Equilibrium studies in the system iron(II) oxide–zirconium oxide. Arch. Eisenhuettenw. 28, 739–743.

Guéneau, C., Dauvois, V., Pérodeaud, P., Gonella, C., Dugne, O., 1998. Liquid immiscibility in a (U, Zr, O) model Corium. J. Nucl. Mater. 254, 158–174.

Guéneau, C., Baichi, M., Labroche, D., Chatillon, C., Sundman, B., 2002. Thermodynamic assessment of the uranium–oxygen system. J. Nucl. Mater. 304, 161–175.

Guinet, P., Vaugoyeau, H., Blum, P.L., 1966. Le Système Uranium-Dioxyde d'Uranium au-dessus de 1130 °C.C.R. Acad. Sci. Paris. Série C 263, 17–20.

Gulliver, G.M., 1922. Metallic Alloys. Griffiths, London.

Hayward, P.J., George, I.M., 1996. Dissolution of UO_2 in molten Zircaloy-4 part 4: phase evolution during dissolution and cooling of 2000–2500 °C specimens. J. Nucl. Mater. 232, 1–12.

Hellmann, S., Nie, M., 10–11/6/1998. Proceedings of the 4th CIT Project Meeting, Pisa, Italy.

Hudon, P., Baker, D.R., 2002. The nature of phase separation in binary oxide melts and glasses. I. Silicate systems. J. Non-Cryst. Solids 303, 299–345.

Journeau, C., Sudreau, F., Magne, S., Cognet, G., 2001. Physico-chemical analyses and solidification path reconstruction of multi-component oxidic melt spreads. Mater. Sci. Eng. 299A, 249–266.

Journeau, C., Piluso, P., Correggio, P., Godin-Jacqmin, L., 2007. The PLINIUS/COLIMA CA-U3 Test on Fission-Product Aerosol Release over a VVER type Corium Pool, Report CEA-R-6160, Saclay, France.

Journeau C., Piluso P., Haquet J.F., Boccaccio E., Saldo V., Bonnet J.M., Malaval S., Carenini L., Brissonneau L., Two-dimensional interaction of Corium with concretes: the VULCANO VB test series. Ann. Nucl. Ener 36(10), 1597–1613.

Juenke, E.F., White, J.F., 1970. Physical–chemical Studies of Clad under Reactor Accident Conditions, Report GEMP–731.

Kleykamp, H., 1997. Phase equilibria in the UO_2-Austenic steel system up to 3000 °C. J. Nucl. Mater. 247, 103–107.

Latta, R.E., Fryxell, R.E., 1970. Determination of solidus–liquidus temperatures in the UO_{2+x} system ($-0.5 < x < 0.2$). J. Nucl. Mater. 35, 195–210.

Levinskii, Yu.V., 1974. P versus T phase diagram of the uranium–oxygen system. Atom. Ener. 37, 1075–1076.

Lungu, S., 1966. Etude des courbes de liquidus et des propriétés thermodynamiques des systèmes SiO_2–ThO_2 et SiO_2–ThO_2–UO_2. J. Nucl. Mater. 19, 155–159.

Manara, D., Ronchi, C., Sheindlin, M., Lewis, M., Brykin, M., 2005. Melting of stoichiometric and hyperstoichiometric uranium dioxide. J. Nucl. Mater. 342, 148–163.

Mezentseva, L.P., Popova, V.F., Almyashev, V.I., Lomanova, N.A., Ugolkov, V.L., Beshta, S.V., Khabenskii, V.B., Gusarov, V.V., 2006. Phase and chemical transformations in the SiO_2–Fe_2O_3(Fe_3O_4) system at various oxygen partial pressures. Russ. J. Inorg. Chem. 51, 118–125.

Mignanelli, M., 2003. ENTHALPY Projet, Private Communication.

Nichols. A.L. (Ed.), 1990. Fission Product Chemistry in Severe Nuclear Reactor Accidents, Specialist's Meeting at JRC-Ispra, 15–17 January 1990, EUR 12989 EN.

Petrov, Yu., Udalov, Yu., Jurek, K., Savazsky, P., Kiselova, M., Selucky, P., Journeau, C., Piluso, P., 2004. New miscibility gap for ex-vessel corium oxide compositions. In: Proceeding of ICAPP'04, Pittsburgh, PA USA, June 13–17.

Petrov, Yu., Udalov, Yu., Subrt, J., Bakardjieva, S., Savazsky, P., Kiselova, M., Selucky, P., Bezdicka, P., Journeau, C., Piluso, P., 2008. Phase equilibrium in melts of the system uranium oxide–iron oxide in air. Glass Phys. Chem. 35, 296–305.

Scheil, E., 1942. Bemerkungen zur schichtkristallbildung. Z. Metallk. 34, 70–73.

Selleby, M, 1997. An assessment of the Ca-Fe-O-Si system. Metall. Mater. Trans. B 28, 577–596.

Sheindlin, M., Heinz, W., Bottomley, D., Knoche, D., Cremer, B., Somers, J., 2004. 11th Symposium on Thermodynamics of Nuclear Materials (11 STNM), Karlsruhe, 6–9 Sept.

Spino, J., Schulz, B., 1981. On the chemical interaction between UO_2 and stainless steel in the liquid state. Rev. Int. Hautes Temp. Réfract. 18, 257–262.